

Stardust Interstellar Preliminary Examination IX: High-speed interstellar dust analog capture in Stardust flight-spare aerogel

F. POSTBERG^{1,2*}, J. K. HILLIER², S. P. ARMES³, S. BUGIEL^{1,4}, A. BUTTERWORTH⁵,
D. DUPIN³, L. A. FIELDING³, S. FUJII³, Z. GAINSFORTH⁵, E. GRÜN^{4,6}, Y. W. LI^{1,4,7},
R. SRAMA¹, V. STERKEN^{1,4,8}, J. STODOLNA⁵, M. TRIELOFF², A. WESTPHAL⁵, C. ACHILLES⁹,
C. ALLEN¹⁰, A. ANSARI¹¹, S. BAJT¹², N. BASSIM¹³, R. K. BASTIEN¹⁰, H. A. BECHTEL¹⁴,
J. BORG¹⁵, F. BRENKER¹⁶, J. BRIDGES¹⁷, D. E. BROWNLEE¹⁸, M. BURCHELL¹⁹,
M. BURGHAMMER²⁰, H. CHANGELA^{21,13}, P. CLOETENS²⁰, A. DAVIS¹¹, R. DOLL²²,
C. FLOSS²², G. FLYNN²³, D. FRANK¹⁰, P. R. HECK²⁴, P. HOPPE²⁵, G. HUSS²⁶, J. HUTH²⁵,
A. KEARSLEY²⁷, A. J. KING¹¹, B. LAI²⁸, J. LEITNER²⁵, L. LEMELLE²⁹, A. LEONARD²²,
H. LEROUX³⁰, R. LETTIERI⁵, W. MARCHANT⁵, L. R. NITTLER³¹, R. OGLIORE²⁶, W. J. ONG²²,
M. C. PRICE¹⁹, S. A. SANDFORD³², J.-A. Sans TRESSARAS²⁰, S. SCHMITZ¹⁶,
T. SCHOONJANS³³, K. SCHREIBER²², G. SILVERSMIT³³, A. SIMIONOVICI³⁴, V. A. SOLÉ²⁰,
F. STADERMANN²², T. STEPHAN¹¹, R. M. STROUD¹³, S. SUTTON²⁸, P. TSOU³⁵,
A. TSUCHIYAMA³⁶, T. TYLICZSZAK¹⁴, B. VEKEMANS³³, L. VINCZE³³, D. ZEVI⁵,
M. E. ZOLENSKY¹⁰, and > 30,000 Stardust@home Dusters³⁷

¹Institut für Raumfahrtssysteme, Universität Stuttgart, Germany

²Institut für Geowissenschaften, Universität Heidelberg, Germany

³Department of Chemistry, University of Sheffield, Sheffield, Yorkshire, UK

⁴Max-Planck-Institut für Kernphysik, Heidelberg, Germany

⁵Space Sciences Laboratory, U.C. Berkeley, Berkeley, California, USA

⁶LASP, University of Colorado at Boulder, Boulder, Colorado, USA

⁷School of Materials Science and Engineering, Harbin Institute of Technology, Harbin, China

⁸IGEP, Technical University of Braunschweig, Braunschweig, Germany

⁹NASA Johnson Space Center, Houston, Texas, USA

¹⁰ARES, NASA Johnson Space Center, Houston, Texas, USA

¹¹University of Chicago, Chicago, Illinois, USA

¹²DESY, Hamburg, Germany

¹³Naval Research Laboratory, Washington, District of Columbia, USA

¹⁴Advanced Light Source, Lawrence Berkeley Laboratory, Berkeley, California, USA

¹⁵IAS Orsay, Orsay, France

¹⁶Institut für Geowissenschaften, Universität Frankfurt am Main, Frankfurt, Germany

¹⁷Space Research Centre, University of Leicester, Leicester, UK

¹⁸Department of Astronomy, University of Washington, Seattle, Washington, USA

¹⁹School of Physical Sciences, University of Kent, Canterbury, UK

²⁰European Synchrotron Radiation Facility, Grenoble, France

²¹George Washington University, Washington, District of Columbia, USA

²²Washington University, St. Louis, Missouri, USA

²³State University of New York Plattsburgh, Plattsburgh, New York, USA

²⁴Robert A. Pritzker Center for Meteoritics and Polar Studies, The Field Museum of Natural History, Chicago, Illinois, USA

²⁵Max-Planck-Institut für Chemie, Mainz, Germany

²⁶University of Hawai'i at Manoa, Honolulu, Hawai'i, USA

²⁷Natural History Museum, London, UK

²⁸Advanced Photon Source, Argonne National Laboratory, Chicago, Illinois, USA

²⁹Ecole Normale Supérieure de Lyon, Lyon, France

³⁰Université des Sciences et Technologies de Lille, Lille, France

³¹Carnegie Institution of Washington, Washington, District of Columbia, USA

³²NASA Ames Research Center, Moffet Field, California, USA

³³University of Ghent, Ghent, Belgium³⁴Institut des Sciences de la Terre, Observatoire des Sciences de l'Univers de Grenoble, Grenoble, France³⁵Jet Propulsion Laboratory, Pasadena, California, USA³⁶Osaka University, Osaka, Japan³⁷Worldwide

*Corresponding author. E-mail: postberg@irs.uni-stuttgart.de

(Received 14 December 2012; revision accepted 24 June 2013)

Abstract—The NASA Stardust mission used silica aerogel slabs to slowly decelerate and capture impinging cosmic dust particles for return to Earth. During this process, impact tracks are generated along the trajectory of the particle into the aerogel. It is believed that the morphology and dimensions of these tracks, together with the state of captured grains at track termini, may be linked to the size, velocity, and density of the impacting cosmic dust grain. Here, we present the results of laboratory hypervelocity impact experiments, during which cosmic dust analog particles (diameters of between 0.2 and 0.4 μm), composed of olivine, orthopyroxene, or an organic polymer, were accelerated onto Stardust flight-spare low-density (approximately 0.01 g cm^{-3}) silica aerogel. The impact velocities ($3\text{--}21 \text{ km s}^{-1}$) were chosen to simulate the range of velocities expected during Stardust's interstellar dust (ISD) collection phases. Track lengths and widths, together with the success of particle capture, are analyzed as functions of impact velocity and particle composition, density, and size. Captured terminal particles from low-density organic projectiles become undetectable at lower velocities than those from similarly sized, denser mineral particles, which are still detectable (although substantially altered by the impact process) at 15 km s^{-1} . The survival of these terminal particles, together with the track dimensions obtained during low impact speed capture of small grains in the laboratory, indicates that two of the three best Stardust candidate extraterrestrial grains were actually captured at speeds much lower than predicted. Track length and diameters are, in general, more sensitive to impact velocities than previously expected, which makes tracks of particles with diameters of $0.4 \mu\text{m}$ and below hard to identify at low capture speeds ($<10 \text{ km s}^{-1}$). Therefore, although captured intact, the majority of the interstellar dust grains returned to Earth by Stardust remain to be found.

INTRODUCTION

In 2000 and 2002, the Stardust mission exposed silica aerogel and aluminum foil collectors, for a total duration of about 200 days, to the stream of interstellar grains sweeping through the solar system (Brownlee et al. 2003). The material was brought back to Earth, together with the grains collected during the flyby of comet Wild 2, in 2006. Here, we report on our work to simulate the capture process by shooting high-speed ($3\text{--}21 \text{ km s}^{-1}$) submicron-sized interstellar dust (ISD) analogs onto Stardust aerogel flight-spare tiles. This enables the investigation of both the morphology of impact tracks as well as structural and chemical modification of projectile and collector material. Such knowledge is an essential prerequisite for the unambiguous identification and investigation of ISD particles brought back to Earth.

In contrast to cometary dust collected at the Wild 2 encounter (e.g., Tsou et al. 2004), which provided typical grain sizes (diameters) of the order of micrometers or tens of micrometers at a constant capture speed of 6.1 km s^{-1} , ISD was expected to be significantly smaller ($0.1\text{--}1 \mu\text{m}$) and faster ($10\text{--}25 \text{ km s}^{-1}$) (Landgraf et al. 1999; Landgraf 2000). Previous laboratory simulations with a light-gas gun only investigated the capture of the larger and slower cometary grains (e.g., Burchell et al. 2008, 2009; Price et al. 2010). The size and speed of most ISD particles are beyond the capabilities of two-stage light-gas guns, which can confer a maximum velocity of approximately 7 km s^{-1} . The complete range of speeds of submicrometer ISD analog particles can only be achieved by an electrostatic Van de Graaff accelerator, such as that operated at the Max-Planck-Institut für Kernphysik in Heidelberg (Mocker et al. 2011), and used for the experiments described here.

THE ELECTROSTATIC DUST ACCELERATOR IN HEIDELBERG

The dust accelerator is a modified Van de Graaff belt generator (Fig. 1), with an adjustable potential of between 0.2 and 2.1 MV. Most (there are minor losses due to imperfect vacuum) of this electrostatic potential can be converted into the kinetic energy of dust particles. To avoid discharging and sparking, the generator is immersed in a protective gas environment (SF₆ and CO₂) in a tank at up to 16 bars. The dust source consists of approximately 0.5 g of a conductive dust sample, stored in an evacuated housing. There, the dust is agitated and positively charged by a strong electric pulse of 10–20 kV. Some of the charged grains leave the source and enter the Van de Graaff, where they are then accelerated. Leaving the accelerator, they pass through the field region of a focusing cathode and enter the beam line. Subsequent measurement of their charge signals, via induction detectors separated by a known distance, allows the speed (v) and mass (m) of individual particles to be determined (Fig. 1). The maximum speed is, in principle, defined by $v = \sqrt{2qU_{acc}/m}$ (q = dust charge, U_{acc} = accelerator potential). For example, a conductively coated mineral particle (with a density of, e.g., 2.5 g cm⁻³) with a diameter of 0.1 μm can achieve a speed of about 50 km s⁻¹, whereas for a 1 μm grain, this decreases to approximately 10 km s⁻¹. Because of the pulsing of the electrode potential inside the dust source, the resulting dust charge fluctuates, leading to variations in speed for particles of the same mass (Fig. 2). The charge detectors can detect maximally charged particles above a diameter of about 30 nm, corresponding to a speed of about 100 km s⁻¹.

Another array of charge detectors and charged plates, the particle selection unit (PSU), selects particles according to a previously defined speed and mass window (Srama and Auer 2008). Only selected particles are permitted to enter the detector chamber, allowing the complete characterization and control of individual dust grains.

EXPERIMENTAL SETUP

The accelerator facility provides high-velocity dust analogs, with complete control of particle size and speed over a wide dynamic range, which can then be shot onto Stardust collector material. The experiments can be carried out using a variety of cosmochemically relevant materials (silicates, sulfides, metals, oxides, carbides). For effective use in the electrostatic accelerator, nonconductive mineral grains must be coated with a thin conducting layer. In this work, the

layer was of either platinum (Hillier et al. 2009) or polypyrrole (e.g., Lascelles and Armes 1995; Goldsworthy et al. 2003; Fujii et al. 2006; Ormond-Prout et al. 2009). Both methods deposit thin conductive layers while particles are suspended in liquid, producing contiguous, or near-contiguous, overlayers with a minimum of aggregation. The thickness of the conductive shells is of the order of 5–10 nm (platinum; Höfer 2010) or 15–20 nm (polypyrrole), respectively.

Accelerator campaigns were successfully carried out in 2010 and 2011 with three different dust materials: orthopyroxene (hereafter OPx, coated $\rho = 3.5$ g cm⁻³), olivine (coated $\rho = 3.4$ g cm⁻³), and poly(bis[4-vinylthiophenyl]sulfide) latex (hereafter PMPV, coated $\rho = 1.33$ g cm⁻³). The olivine and PMPV were coated with polypyrrole (Figs. 3a and 3b) and the OPx grains with platinum (Fig. 4). A typical platinum layer about 5 nm thick (Höfer 2010) modified the bulk density of the particles, to an extent dependent on the original size of the particle. However, in the framework of this investigation, it is only significant for particles below 0.2 μm in diameter (where the density is increased by more than 25% by Pt coating). The particles were shot within several narrow speed and size windows (e.g., 14–16 km s⁻¹, 0.35–0.41 μm). All particle diameters given in this work are equivalent diameters of an idealized spherical particle.

For each set of parameters (Table 1), about 50 particles were accelerated and selected. Square-cut aerogel pieces with a surface area of about 2 cm² were mounted into the beam line. The total beam line and housing of the aerogel mounting were subsequently evacuated to a pressure of 10⁻⁷ to 10⁻⁶ mbar. The housing was equipped with a glass window that allowed adjustment of the position and orientation of the tile. Aerogel properties, generally controlled by density, can be quite variable. To remove systematic uncertainties due to differences in an aerogel batch, a single aerogel tile for each set of shots was used. To distinguish among the tracks, the zenith (incidence) angle (45°) was held constant and the tile rotated through different azimuth angles in increments of 30° or 45°. The different populations are thus readily distinguishable within a single aerogel tile.

The following flight-spares collector tiles were used

OPx: 159 5A #1

PMPV: 201 4F #2 & 159 5A #1

Olivine: E250 9f #1

Owing to technical issues with the PSU, full dynamic parameters could only be obtained for a fraction of the particles that were originally accelerated. The diameter and velocity ranges of particles are shown in Table 1.

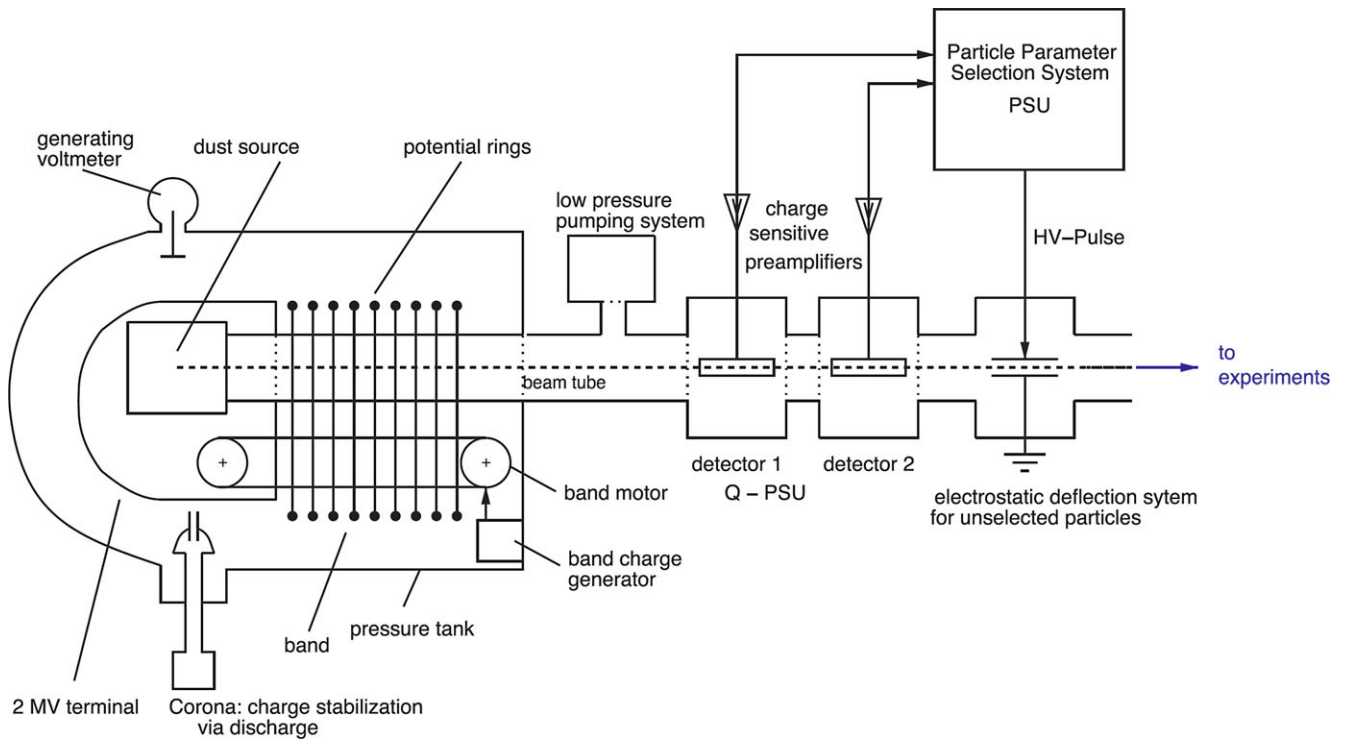


Fig. 1. Schematic of the Heidelberg dust accelerator (Mocker et al. 2011).

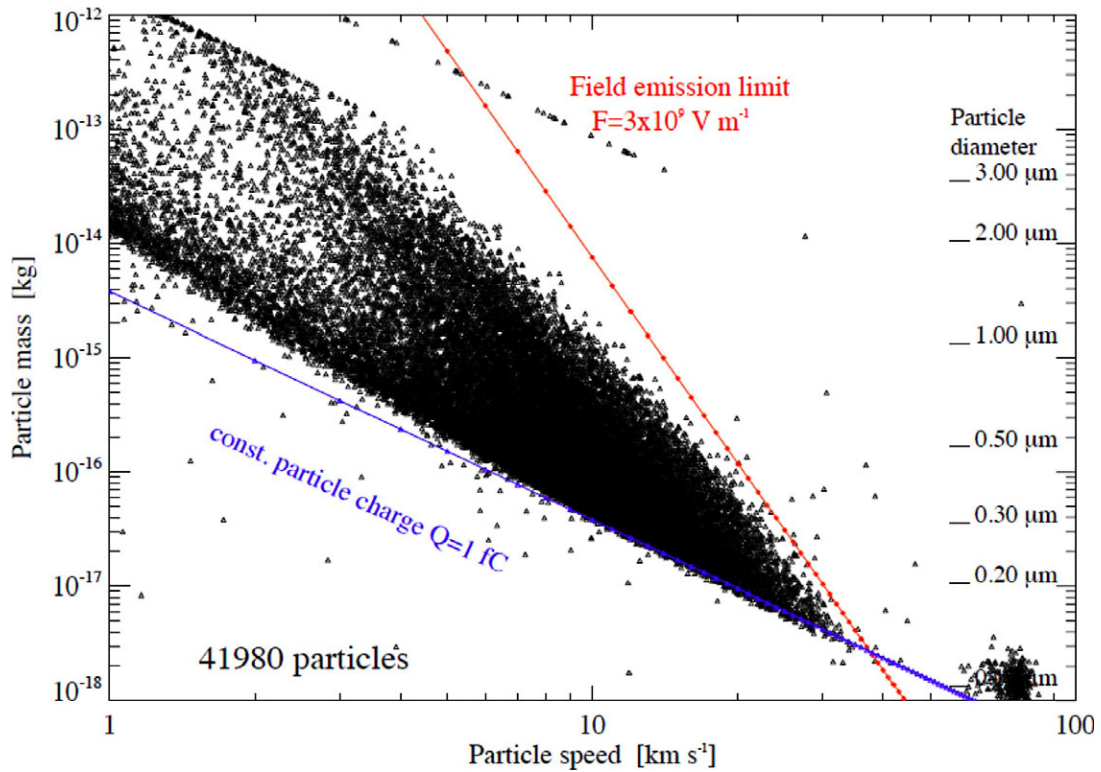


Fig. 2. Particle mass and diameter versus speed distribution of accelerated platinum-coated orthopyroxene particles (assuming a mean $\rho = 3.5 \text{ g cm}^{-3}$) used in the Stardust aerogel campaign at an accelerator potential of 1.8 MV. Adjustment of the potential shifts the distribution to the right or left.

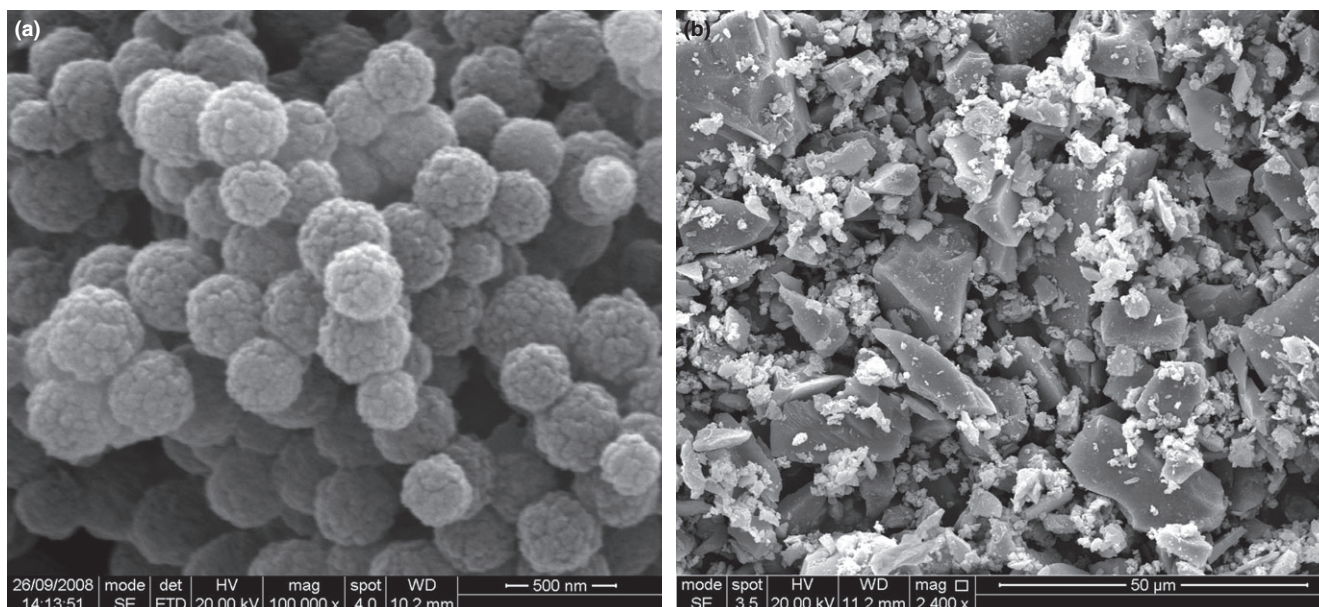


Fig. 3. a) Scanning electron microscope (SEM) image of poly(bis[4-vinylthiophenyl]sulfide) latex particles coated with polypyrrole. As can be seen from the image, the size distribution of these synthetic spherical particles is quite narrow (diameters approximately 0.2–0.5 μm). The scale bar is 500 nm. b) SEM image of Olivine particles coated with polypyrrole. The scale bar is 50 μm .

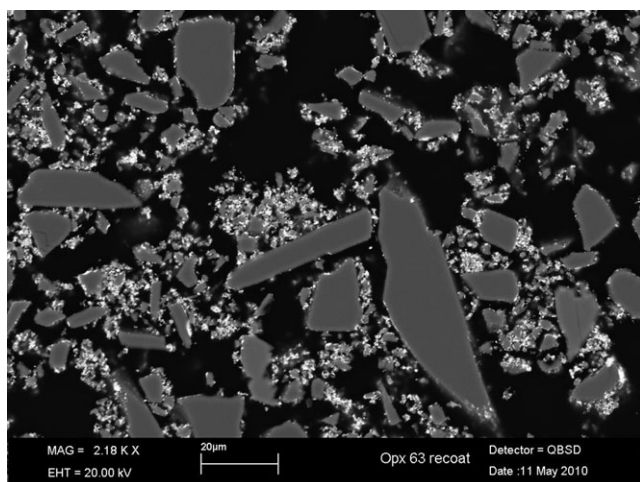


Fig. 4. Scanning electron microscope image (from Höfer 2010) of orthopyroxene particles coated with platinum. This image was produced from a sample of dust set in resin and then milled, resulting in an apparently inhomogeneous coating. In reality, the larger particles are believed to have a coating similar in distribution and coverage to the smaller particles. The method used to produce the particles (grinding and milling from a larger sample) results in a far wider distribution of particle sizes, similar to that of the olivine (Fig. 3b), when compared with that observed for the synthetic polypyrrole-coated poly(bis[4-vinylthiophenyl]sulfide) latex particles (Fig. 3a). The scale bar is 20 μm .

TRACK IDENTIFICATION AND INVESTIGATION

The tiles were initially surveyed with an optical microscope to identify impacts (Fig. 5a). SEM imaging

was also sometimes used (Fig. 5b) to image track mouths, but was not used to survey the tile to identify tracks. The maximum track diameters close to the entrance hole at the aerogel surface were measured optically at high magnification with an encoded stage with 0.5 μm precision. In general, only a fraction of the initially fired particles could be recovered in the aerogel. This was partly due to a misadjusted beam line, which was wider than the target area, and also technical problems with the PSU. Track sizes below 2 μm could only be identified with great difficulty. Therefore, it is quite likely that only the largest of these small tracks have been found for the lower velocity impacts.

Subsequently, typical tracks in picokeystones (extracted subvolumes of an aerogel tile that contain a single track, e.g., Westphal et al. 2010; Frank et al. 2013) were extracted and analyzed with the scanning transmission X-ray microscopy (STXM) beam line 11.0.2 at the Advanced Light Source, Lawrence Berkeley National Laboratory, in Berkeley, CA. This beam line uses a zone plate and order-sorting aperture to focus a monochromatic X-ray beam to spot sizes as small as 15 nm.

RESULTS

For close investigation, picokeystones of typical tracks have been extracted for each speed regime. STXM images taken from these are shown in Figs. 6–10. For the 3 km s^{-1} picokeystone (Fig. 11), only an optical image could be obtained. Not only the

Table 1. Properties of dust particles that have been evaluated for this work. For the equivalent diameter a spherical particle is assumed, which is inferred from the selected particle mass. For OPx and olivine, this is of course an unrealistic idealization (see Fig. 3). For 0.11–0.13 μm OPx, all tracks were too small to be identified with an optical microscope.

Speed/equivalent diameter	2.5–3.5 km s^{-1}	5.5–6.5 km s^{-1}	9–11 km s^{-1}	14–16 km s^{-1}	19–21 km s^{-1}
0.11–0.13 μm				(OPx)	
0.19–0.24 μm			OPx	OPx	OPx
0.32–0.38 μm			PMPV	PMPV	PMPV
0.36–0.44 μm	Olivine	Olivine	Olivine	OPx ^a	

^aAfter density correction for the platinum coating, the average equivalent diameter goes down to 0.37 μm .

OPx, orthopyroxene; PMPV, poly(bis[4-vinylthiophenyl]sulfide) latex.

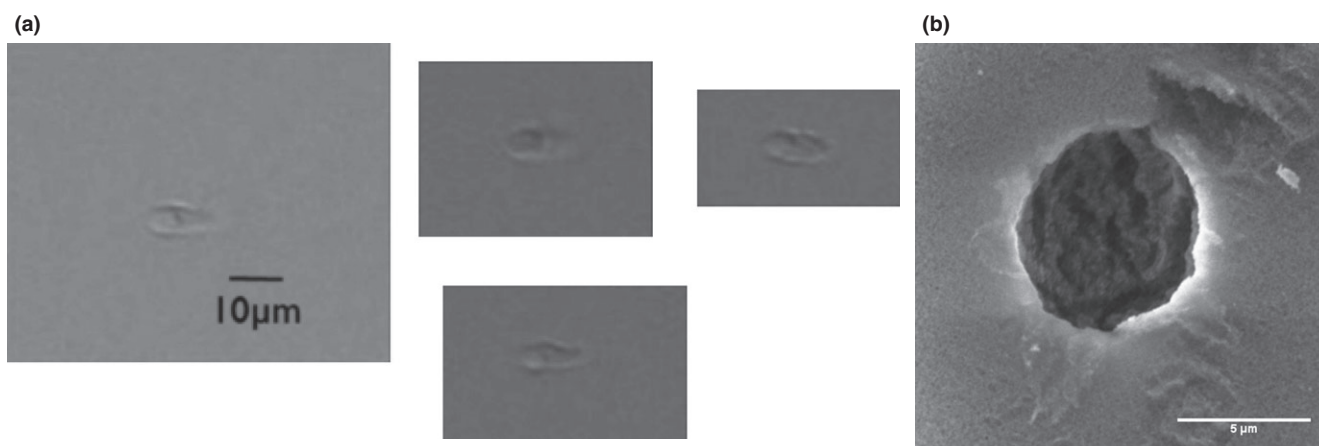


Fig. 5. a) Track entrance holes where orthopyroxene particles ($v = 20 \pm 1 \text{ km s}^{-1}$) penetrate the aerogel surface as seen in a survey with the optical microscope. The image has been contrast enhanced for publication. At these high speeds, the tracks are fairly easy to identify. The maximum diameter of the track at its entry point is one key parameter for this work. b) A scanning electron microscope image of the track entrance hole of a 20 km s^{-1} poly(bis[4-vinylthiophenyl]sulfide) latex particle, clearly showing the porous nature of the aerogel target. The scale bar is 5 μm .

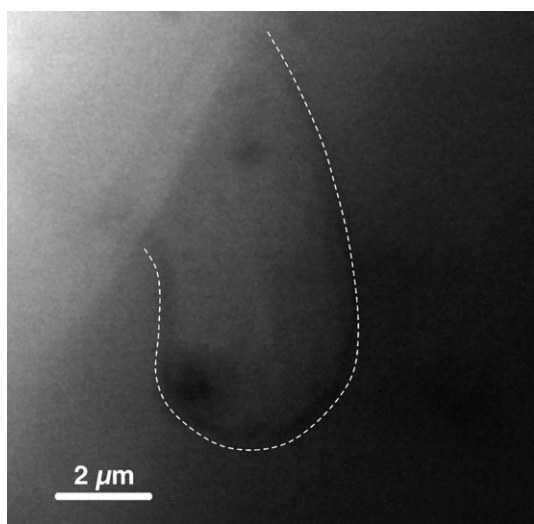


Fig. 6. 1304 eV scanning transmission X-ray microscopy image of a track (outlined) in a picokeystone from a 0.21 μm orthopyroxene projectile captured at 20 km s^{-1} . Maximum diameter 4.5 μm , depth 9 μm .

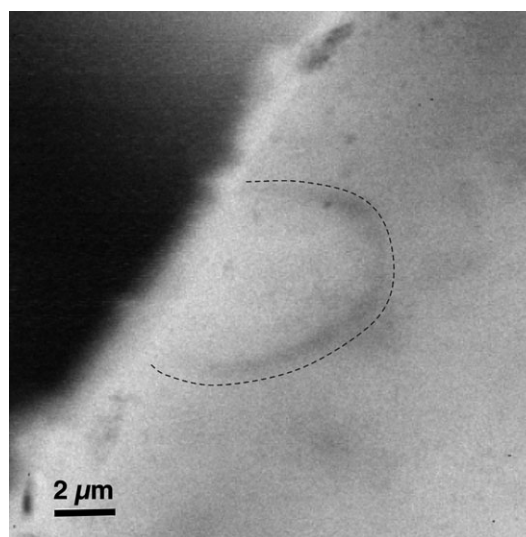


Fig. 7. 853 eV scanning transmission X-ray microscopy image of a track (outlined) in a picokeystone from a 0.35 μm poly(bis[4-vinylthiophenyl]sulfide) latex projectile captured at 15 km s^{-1} . Maximum diameter 6 μm , depth 9 μm .

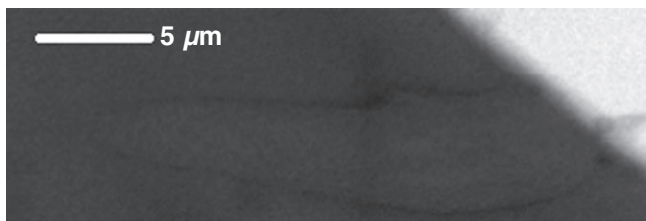


Fig. 8. 1304 eV scanning transmission X-ray microscopy image of a track in a picokeystone from a 0.37 μm orthopyroxene projectile captured at 15 km s⁻¹. Maximum diameter 5 μm, depth 23 μm.

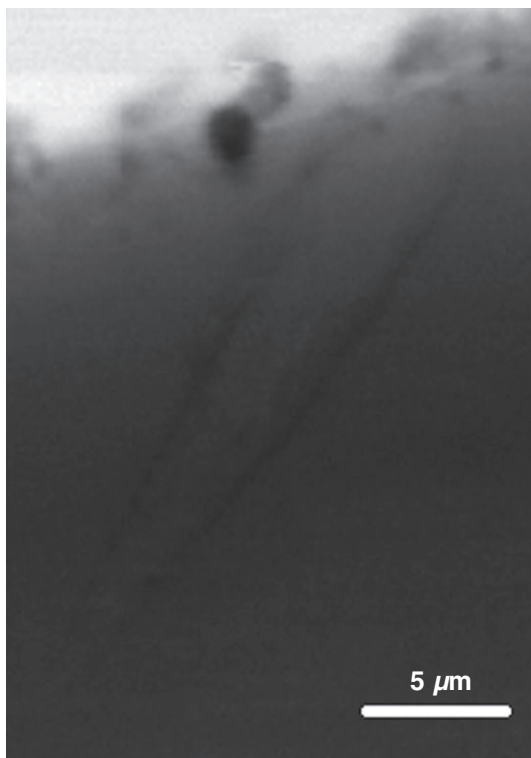


Fig. 9. 1000 eV scanning transmission X-ray microscopy image of a track in a picokeystone from a 0.40 μm olivine projectile captured at 10 km s⁻¹. Maximum diameter 4.5 μm, depth 22 μm.

maximum track diameters but the track morphology as a whole varies with capture speed. This is different from the cometary aerogel collector where three track types were identified at a single impact speed of 6.1 km s⁻¹ (Hörz et al. 2006, 2009; Burchell et al. 2008).

In the cometary dust case, these track types were long and narrow (type A), initially bulbous with some narrow tracks beneath the bulb (type B), or purely bulbous (type C). The differences were associated with the structure and composition of the impacting cometary dust particles (e.g., see Kearsley et al. 2009, 2012).

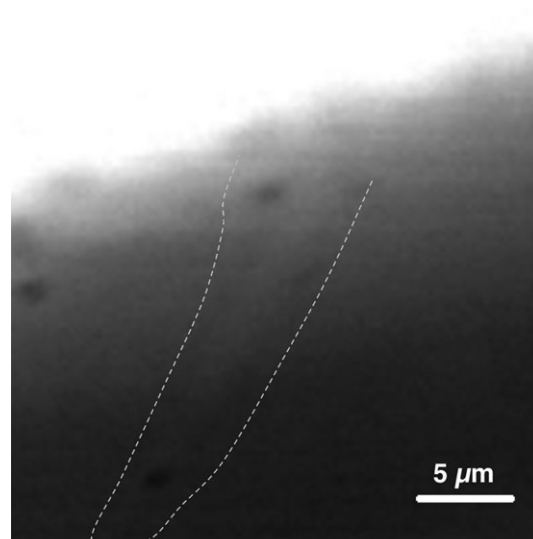


Fig. 10. 1000 eV scanning transmission X-ray microscopy image of a track (outlined) in a picokeystone from a 0.40 μm olivine projectile captured at 6 km s⁻¹. Maximum diameter 3 μm, depth 18 μm.

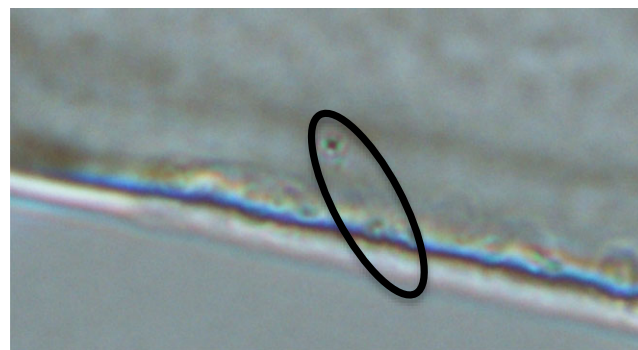


Fig. 11. Optical image of a track in a picokeystone from a 0.40 μm olivine projectile captured at 3 km s⁻¹. Maximum diameter 1.5 μm, depth 14 μm.

By contrast, in this new calibration, the track morphology is speed dependent, even for a single particle type. Although high-speed impacts above 15 km s⁻¹ mostly form bulbous tracks, the track shapes become more linear at low capture speed and often are similar, although much smaller, to the “whisker track” type A tracks observed in Stardust cometary samples.

Terminal particles can be identified in tracks after shots at 3, 6, 10, and 15 km s⁻¹. At 20 km s⁻¹, only an enhanced concentration of (probably recondensed) residue of the OPx particle could be found at the end of the track. STXM Mg-K near-edge absorption fine structure spectroscopy of a 0.37 μm OPx shot at 15 km s⁻¹ (Fig. 12) shows that the particle has been altered during capture. The Mg content has been reduced from an initial concentration of 19% to 5%,

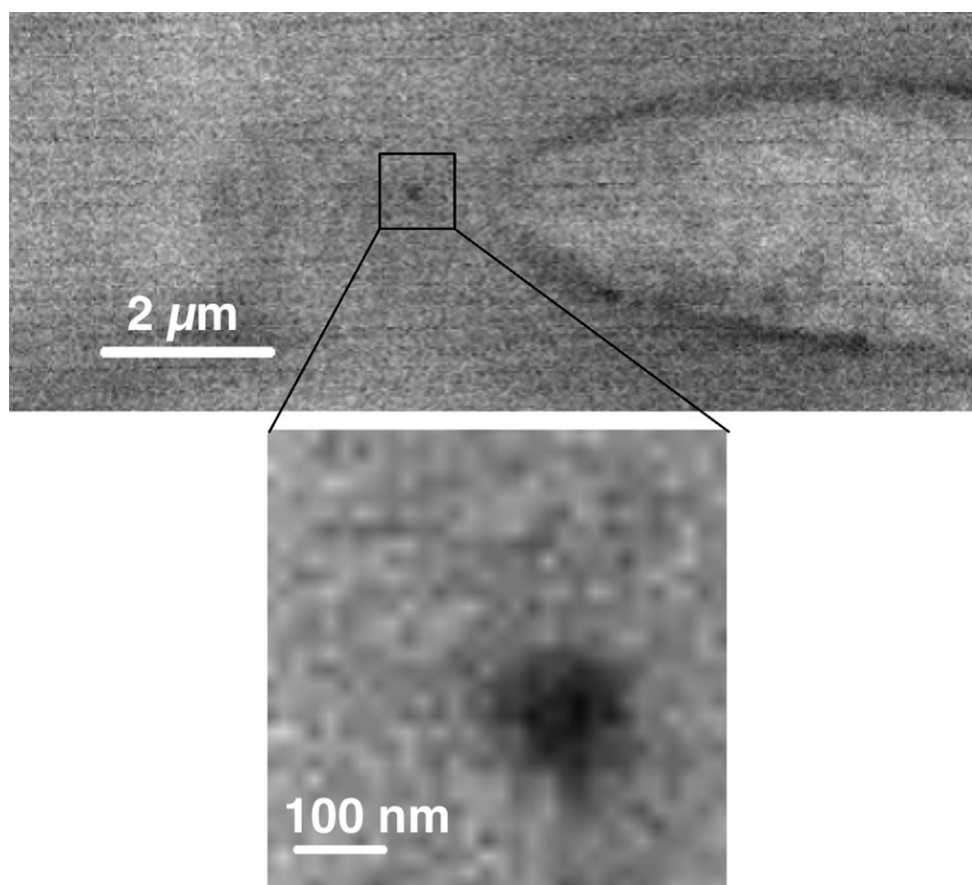


Fig. 12. 1304 eV scanning transmission X-ray microscopy image of a terminal particle. Orthopyroxene impactor size: $0.37\ \mu\text{m}$, capture speed: $15\ \text{km s}^{-1}$ (same track as in Fig. 8). Mg-K near-edge absorption spectroscopy indicates a reduced Mg content due to mixing with aerogel.

which indicates heavy mixing with aerogel. This is consistent with the almost spherical shape of the terminal particle and its reduction in size (to $\approx 0.15\ \mu\text{m}$), both indicating at least partial melting.

We observed a large dispersion (see, e.g., the error bars in Fig. 13) in maximum track diameters, even within the same dynamical parameter window. This observation is consistent with the large dispersions in track morphology that have been observed consistently in hypervelocity capture experiments in aerogel (e.g., Burchell et al. 2008). This is probably due to the drastically varying particle shapes (Fig. 4) and the stochastic variations of density and surface roughness of aerogel.

Figure 13 shows the maximum diameter of tracks close to the track mouths as a function of particle size and speed for OPx, olivine, and PMPV. Based on simple physical arguments, Dominguez (2005) predicted a track diameter dependence with velocity of $v^{1/2}$. However, the present study implies a much steeper curve with an exponent of about unity up to $15\ \text{km s}^{-1}$ and an even higher exponent at speeds above

$15\ \text{km s}^{-1}$. Therefore, the tracks obtained with speeds above about $10\ \text{km s}^{-1}$ are larger than previously expected, whereas below about $10\ \text{km s}^{-1}$, track sizes are smaller.

Although their mass is more than three times greater, OPx particles generate only slightly wider tracks than PMPV particles of similar size (Fig. 14). Particle density clearly only has a minor influence on track width. This is consistent with expectations: the local track diameter is, in principle, less dependent on density than on the geometrical properties of the particle, while track length is also dependent on particle mass and density.

DISCUSSION

Implications for the Stardust Extraterrestrial Candidate Particles

For the first time, it has been shown experimentally that cores of mineral grains below $0.5\ \mu\text{m}$ survive aerogel capture at a speed of $15\ \text{km s}^{-1}$. Above

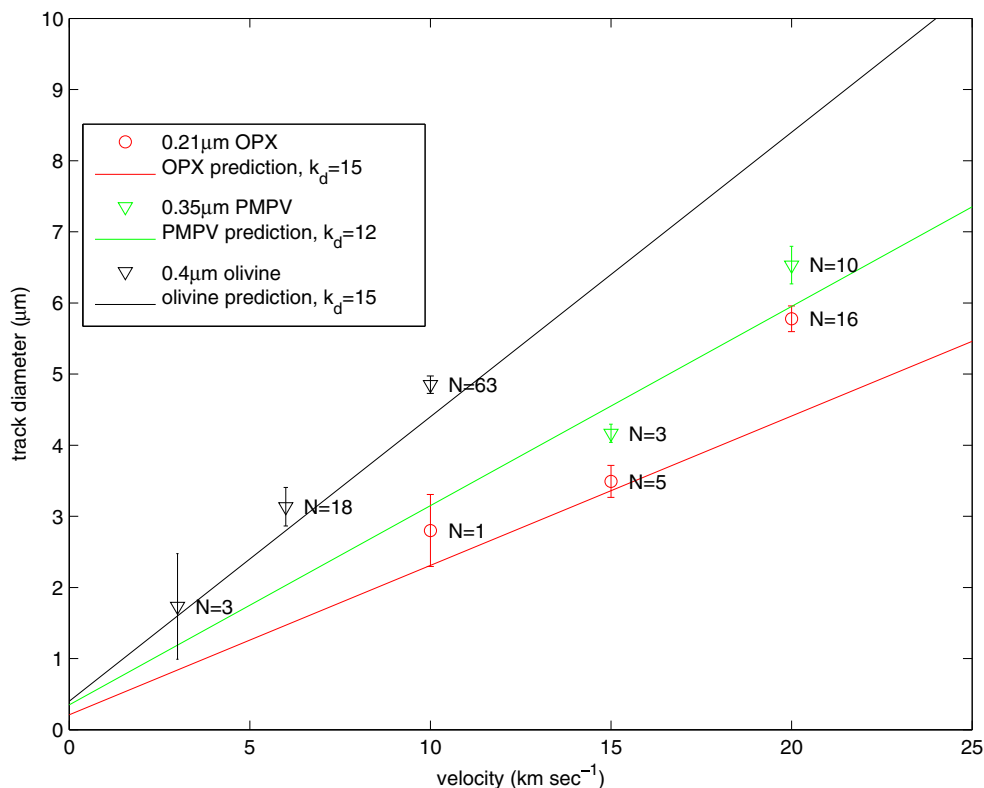


Fig. 13. Maximum track diameter close to the entrance hole as a function of projectile velocity. The linear fitting function used here is $D_{\text{track}} = D_{\text{particle}} (K_d (v/15 \text{ km s}^{-1}) + 1)$. Above 15 km s^{-1} , the function is probably steeper than linear. Note that track diameters below $3 \mu\text{m}$ could only be identified with great difficulty. Therefore, it is likely that the low velocity values at 3 and 6 km s^{-1} are an upper limit of the real average entrance hole diameter. The statistical error bars are defined as the $\text{sqrt}(\text{var}(\text{data})/N)$. To avoid unrealistic track diameters at low speeds, we assume that track entrance hole and particle diameter are identical at (close to) zero velocity.

10 km s^{-1} melting and severe mixing with aerogel, even by refractory minerals, can be expected. At 20 km s^{-1} capture speed, no terminal particles were observed in our experiments. Therefore, Stardust ISD particles with a diameter below $0.5 \mu\text{m}$ and capture speeds above 15 km s^{-1} cannot be expected to be captured intact. Stardust extraterrestrial candidate “Sorok” (Track 40, curation number I1003,1,40) shows the most similar track morphology (Butterworth et al. 2014), without a terminal particle, to the analog shots at $15\text{--}20 \text{ km s}^{-1}$. Although all dimensions of Track 40 are larger, its bulbous shape and aspect ratio (Fig. 15) indicate capture at a similarly high speed. Using our laboratory calibration (Fig. 14), the observed maximum track diameter agrees best with an equivalent particle diameter of about $0.9 \mu\text{m}$.

The intact terminal extraterrestrial candidate particles Orion (Track 30, curation number I1043,1,30) and Hylabrook (Track 34, curation number I1047,1,34) only show either weak alteration or no signs of alteration (e.g., Butterworth et al. 2014), which is indicative of a

much lower capture speed. Their well-preserved state and the thin, elongated track shapes are strongly indicative of capture velocities below 10 km s^{-1} .

This is in contrast to ISD modeling, which predicts impact speeds far above 10 km s^{-1} for astronomical silicate particles with diameters of $1 \mu\text{m}$ or higher (Landgraf et al. 1999; Sterken et al. 2014). However, if particles are more sensitive to solar radiation pressure, they should be decelerated substantially during the Stardust collection period (Sterken et al. 2014). In fact, this is the only way to reconcile the low capture speeds inferred in this work with the current understanding of the ISD flux through the solar system. The most effective way to increase particle sensitivity to radiation pressure is either to change their surface properties (e.g., albedo, composition) or to lower their density. The latter possibility is consistent with the low densities of the terminal particles reported by Butterworth et al. (2014). Analog shots with low-density dust are scheduled for 2013 and will help verify this hypothesis.

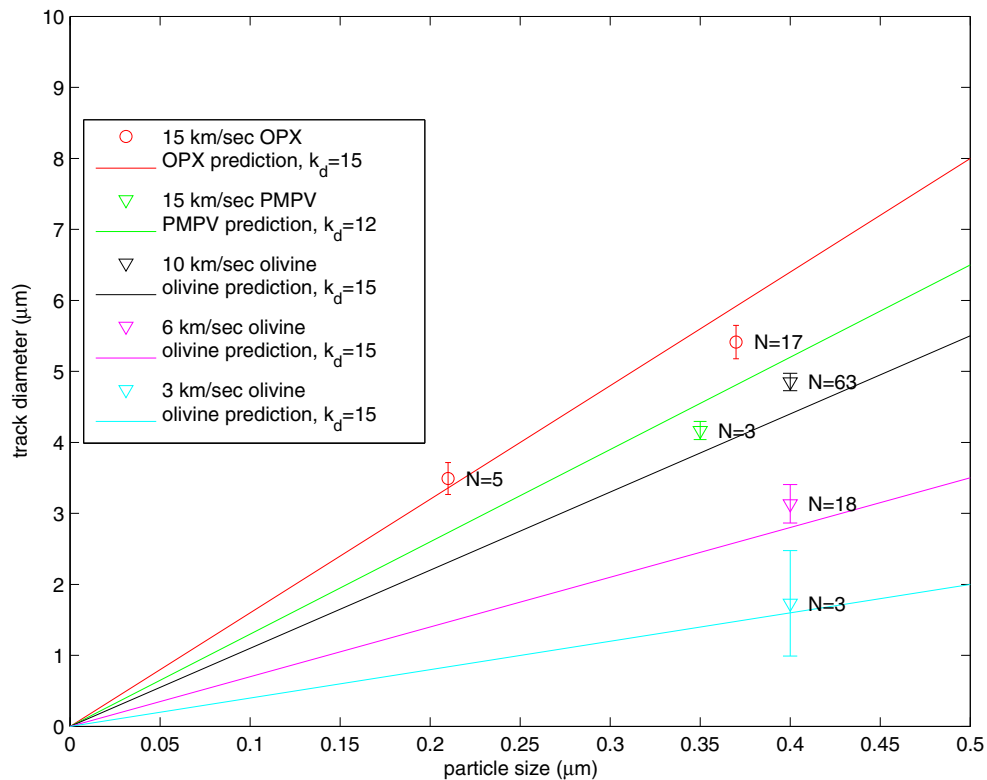


Fig. 14. Maximum track diameter close to the entrance hole as a function of particle diameter for different materials and velocities. The statistical error bars are defined as the sqrt ($\text{var}(\text{data})/N$). A linear fit was chosen based on previous work (e.g., Burchell et al. 2008).

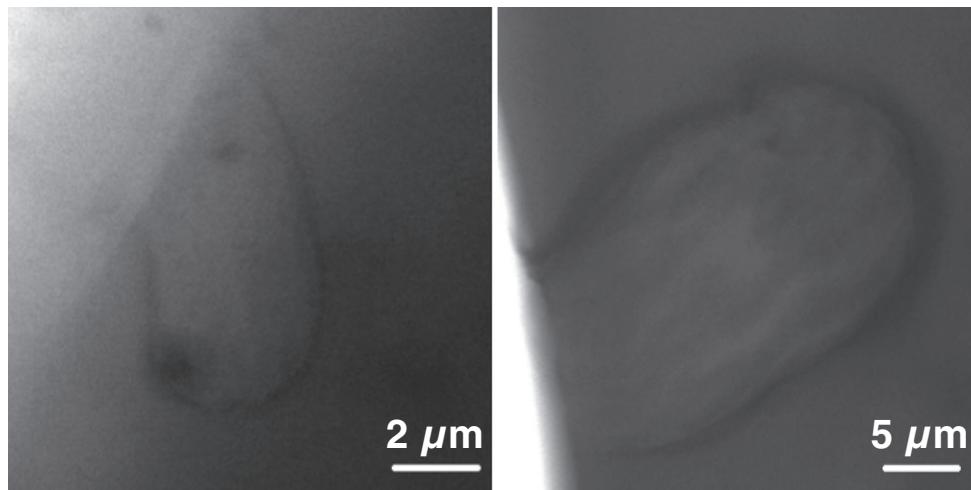


Fig. 15. Comparison of the STXM Mg map (left, 1304 eV) of an orthopyroxene dust particle ($d \sim 0.37 \mu\text{m}$) shot at $20 \pm 1 \text{ km s}^{-1}$ onto aerogel and a scanning transmission X-ray microscopy C map (right, 330 eV) of extraterrestrial candidate Sorok (Butterworth et al. 2014). Although smaller, the overall morphology of the analog track is very similar to that of Sorok.

Implications for the Total Number of Particles in the Stardust ISD Collection

The three best extraterrestrial candidate tracks found in Stardust aerogel collectors so far indicate

diameters of the order of $1 \mu\text{m}$ or larger (Westphal et al. 2014). Measurements by the Ulysses spacecraft (Krüger et al. 2007) and numerical modeling (Landgraf et al. 1999; Landgraf 2000) imply that the flux of ISD particles through the solar system is highest for particles

with diameters of about 0.5 μm . Recent modeling by Sterken et al. (2014) finds that the vast majority of ISD grains captured by Stardust should have even lower diameters (0.2–0.5 μm .) Over 100 ISD grains are predicted to have been brought back to Earth in the Stardust aerogel collectors, most of them with sizes in the order of 0.2 μm . Sterken et al. (2014) show that capture speeds of 3–7 km s^{-1} on both sides of the collector could indeed be expected for most particles below 0.5 μm in size. However, particles in this size regime have not yet been found in the Stardust collectors. One possible reason might be that they have been overlooked. Our analog shots show that 0.4 μm particles with capture speeds of 6 km/s and below may already have a low detection efficiency and 0.2 μm particles are almost undetectable using optical microscopy. In this speed regime, the average entrance hole diameter of the track drops below 2 μm , corresponding to the threshold below which detection efficiencies by the Stardust@home participants (Westphal et al. 2014) are not well constrained.

The three relatively large extraterrestrial candidate tracks identified so far might be just the tip of the iceberg. The large fluence of small craters in the collector foils, identified by SEM scanning (Stroud et al. 2014) supports this idea. Although many of these craters are clearly due to secondary impacts from solar panel ejecta, at least four are of potential interstellar origin.

SUMMARY

Shots with a variety of ISD analogs have been carried out at the electrostatic dust accelerator in Heidelberg. Particles between 0.2 and 0.4 μm in size were fired onto Stardust flight-spare aerogel at velocities ranging from 3 to 21 km s^{-1} . The captured particles and their tracks in aerogel have been investigated with optical microscopy and X-ray spectroscopy.

Mineral particles survive aerogel capture at impact speeds of up to 10 km s^{-1} , but can become modified during this process (Zolensky et al. 2006). At 15 km s^{-1} , the terminal particle indicates at least partial melting and substantial mixing with aerogel. However, by this speed the low-density, nonrefractory PMPV particles produced no identifiable terminal particles. At 20 km s^{-1} , no terminal particle could be identified with any material. Maximum track diameters scale approximately linearly with capture speed from 3 to 15 km s^{-1} , although at velocities higher than 15 km s^{-1} there are indications for this scaling becoming nonlinear. Track shapes are, in general, elongated at capture speeds of 10 km s^{-1} and below and become bulbous at 15–20 km s^{-1} . The average maximum track

width of 0.4 μm particles drops below 3 μm at 6 km s^{-1} , which is already near the detection threshold for the stardust@home participants (Westphal et al. 2014). Particles with a diameter of 0.2 μm are well below the detection threshold at that speed. Recent modeling (Sterken et al. 2014) indicates that most particles in the size regime of the ISD flux maximum (0.2–0.5 μm) were probably captured at velocities below 6 km/s on both sides of the collector. We conclude that small ISD particles brought to Earth intact by Stardust, which probably constitute the majority, have not yet been identified.

Comparison of the analog shots with the three best micron-sized, extraterrestrial candidates that have currently been identified in the Stardust aerogel collectors (Westphal et al. 2014) shows that only one was captured at the speed (15–25 km s^{-1}) predicted for ISD of this size and evaporated during that process. The other two were captured intact at speeds below 10 km s^{-1} , which can be reconciled with the current understanding of the ISD flux (Sterken et al. 2014) if the particles are low density, or more sensitive in other ways to decelerating radiation pressure than previously modeled (Landgraf et al. 1999). The large difference in the capture speeds of the three best ISD candidates is remarkable and cannot be explained with different collection periods alone. It implies substantially different particle characteristics, with diverging surface properties and/or densities. It seems possible that the compactness of the extraterrestrial candidates governs their fate after capture with, rather counterintuitively, the compact particles being evaporated, while the more fragile particles remain more or less intact due to their lower capture speed. However, more potential ISD grains have to be found before reliable conclusions can be drawn.

Acknowledgments—The ISPE consortium gratefully acknowledge the NASA Discovery Program for Stardust, the fourth NASA Discovery mission. AJW, ALB, ZG, RL, DZ, WM and JVK were supported by NASA grant NNX09AC36G. We thank Steve Boggs for astrophysical soft x-ray spectra. RMS, HCG and NDB were supported by NASA grant NNH11AQ61I. The Advanced Light Source is supported by the Director, Office of Science, Office of Basic Energy Sciences, of the U.S. Department of Energy under Contract No. DE-AC02-05CH11231. Use of the National Synchrotron Light Source, Brookhaven National Laboratory, was supported by the U.S. Department of Energy, Office of Science, Office of Basic Energy Sciences, under Contract No. DE-AC02-98CH10886.

FP, JKH, RS and MT acknowledge funding by DFG special priority program 1385 “The First 10 Million years of the Solar System” and the support by Klaus Tschira Stiftung GmbH.

Editorial Handling—Dr. Christian Koeberl

REFERENCES

- Brownlee D. E., Tsou P., Anderson J. D., Hanner M. S., Newburn R. L., Sekanina Z., Clark B. C., Hörz F., Zolensky M. E., Kissel J., McDonnell J. A. M., Sandford S. A., and Tuzzolino A. J. 2003. Stardust: Comet and interstellar dust sample return mission. *Journal of Geophysical Research* 108:1, doi:10.1029/2003JE002087.
- Burchell M. J., Fairey S. A. J., Wozniakewicz P., Brownlee D. E., Hörz F., Kearsley A. T., See T. H., Tsou P., Westphal A., Green S. F., Trigo-Rodríguez J. M., and Dominguez G. 2008. Characteristics of cometary dust tracks in Stardust aerogel and laboratory calibrations. *Meteoritics & Planetary Science* 43:23–40, doi:10.1111/j.1945-5100.2008.tb00608.x.
- Burchell M. J., Foster N. J., Ormond-Prout J., Dupin D., and Armes S. P. 2009. Extent of thermal ablation suffered by model organic microparticles during aerogel capture at hypervelocities. *Meteoritics & Planetary Science* 44:1407–1420, doi:10.1111/j.1945-5100.2009.tb01182.x.
- Butterworth A., Westphal A. J., Tyliczszak T., Gainsforth Z., Stodolna J., Frank D. R., Allen C., Anderson D., Ansari A., Bajt S., Bastien R. S., Bassim N., Bechtel H. A., Borg J., Brenker F. E., Bridges J., Brownlee D. E., Burchell M., and Burghammer M., Changela H., Cloetens P., Davis A. M., Doll R., Floss C., Flynn G., Grün E., Heck P. R., Hillier J. K., Hoppe P., Hudson B., Huth J., and Hvide B., Kearsley A., King A. J., Lai B., Leitner J., Lemelle L., Leroux H., Leonard A., Lettieri R., Marchant W., Nittler L. R., Ogliore R., Ong W. J., Postberg F., Price M. C., Sandford S. A., Sans Tresseras J., Schmitz S., Schoonjans T., Silversmit G., Simionovici A. S., Sole V. A., Srama R., Stephan T., Sterken V. J., Stroud R. M., Sutton S., Trieloff M., Tsou P., Tsuchiyama A., Vekemans B., Vincze L., Korff J. V., Wordsworth N., Zevin D., and Zolensky M. E., and >30,000 Stardust@home dusters. 2014. Stardust Interstellar Preliminary Examination IV: Scanning Transmission X-ray Microscopy analyses of impact features in the Stardust Interstellar Dust Collector. *Meteoritics & Planetary Science*, doi:10.1111/maps.12220.
- Dominguez G. 2005. Fluorescent aerogels for the capture and identification of hypervelocity extra-terrestrial particles. Ph.D. thesis, University of California, Berkeley, California.
- Frank D. R., Westphal A. J., Zolensky M. E., Gainsforth Z., Butterworth A. L., Bastien R. K., Allen C., Anderson D., Ansari A., Bajt S., Bassim N., Bechtel H. A., Borg J., Brenker F. E., Bridges J., Brownlee D. E., Burchell M., Burghammer M., Changela H., Cloetens P., Davis A. M., Doll R., Floss C., Flynn G., Grün E., Heck P. R., Hillier J. K., Hoppe P., Hudson B., Huth J., Hvide B., Kearsley A., King A. J., Lai B., Leitner J., Lemelle L., Leroux H., Leonard A., Lettieri R., Marchant W., Nittler L. R., Ogliore R., Ong W. J., Postberg F., Price M. C., Sandford S. A., Tresseras J.-A. S., Schmitz S., Schoonjans T., Silversmit G., Simionovici A. S., Sole V. A., Srama R., Stephan T., Sterken V. J., Stroud R. M., Sutton S., Trieloff M., Tsou P., Tsuchiyama A., Tyliczszak T., Vekemans B., Vincze L., Von Korff J., Wordsworth N., Zevin D., and >30,000 Stardust@home dusters. 2013. Stardust Interstellar Preliminary Examination II: Curating the Stardust interstellar dust collector: Picokeystones, the Stardust interstellar preliminary exam (ISPE), and beyond. *Meteoritics & Planetary Science*, doi:10.1111/maps.12147.
- Fujii S., Armes S. P., Jeans R., Devonshire R., Warren S., McArthur S. L., Burchell M. J., Postberg F., and Srama R. 2006. Synthesis and characterization of polypyrrole-coated sulfur-rich latex particles: New synthetic mimics for sulfur-based micrometeorites. *Chemical Materials* 18:2758–2765, doi:10.1021/cm0601741.
- Goldsworthy B. J., Burchell M. J., Cole M. J., Armes S. P., Khan M. A., Lascelles S. F., Green S. F., McDonnell J. A. M., Srama R., and Bigger S. W. 2003. Time of flight mass spectrometry of ions in plasmas produced by hypervelocity impacts of organic and mineralogical microparticles on a cosmic dust analyser. *Astronomy & Astrophysics* 409:1151–1167.
- Hillier J. K., Sestak S., Green S. F., Postberg F., Srama R., and Trieloff M. 2009. The production of platinum-coated silicate nanoparticle aggregates for use in hypervelocity impact experiments. *Planetary and Space Science* 57:2081–2086, doi:10.1016/j.pss.2009.09.019.
- Höfer C. 2010. Präparation und Analyse von Analogmaterial für extraterrestrischen Staub. Bachelorarbeit, Universität Heidelberg, Germany.
- Hörz F., Bastien R., Borg J., Bradley J. P., Bridges J. C., Brownlee D. E., Burchell M. J., Chi M., Cintala M. J., Dai Z. R., Djouadi Z., Dominguez G., Economou T. E., Fairey S. A. J., Floss C., Franchi I. A., Graham G. A., Green S. F., Heck P., Hoppe P., Huth J., Ishii H., Kearsley A. T., Kissel J., Leitner J., Leroux H., Marhas K., Messenger K., Schwandt C. S., See T. H., Snead C., Stadermann F. J. I., Stephan T., Stroud R., Teslich N., Trigo-Rodríguez J. M., Tuzzolino A. J., Troadec D., Tsou P., Warren J., Westphal A., Wozniakewicz P., Wright I., and Zinner E. 2006. Impact features on the Stardust collector and implications for Wild 2 coma dust. *Science* 314:1716–1719, doi: 10.1126/science.1135705.
- Hörz F., Cintala M. J., See T. H., and Nakamura-Messenger K. 2009. Penetration tracks in aerogel produced by Al₂O₃ spheres. *Meteoritics & Planetary Science* 44:1243–1264, doi:10.1111/j.1945-5100.2009.tb01221.x.
- Kearsley A. T., Burchell M. J., Price M. C., Graham G. A., Wozniakewicz P. J., Cole M. J., Foster N. J., and Teslich N. 2009. Interpretation of Wild 2 dust fine structure: Comparison of Stardust aluminium foil craters to the three dimensional shape of experimental impacts by artificial aggregate particles and meteorite powders. *Meteoritics & Planetary Science* 44:1489–1510, doi:10.1111/j.1945-5100.2009.tb01188.x.
- Kearsley A. T., Burchell M. J., Price M. C., Cole M. J., Wozniakewicz P. J., Ishii H. A., Bradley J. P., Fries M., and Foster N. J. 2012. Experimental impact features in Stardust aerogel: How track morphology reflects particle structure, composition and density. *Meteoritics & Planetary Science* 47:737–762, doi:10.1111/j.1945-5100.2012.01363.x.

- Krüger H., Landgraf M., Altobelli N., and Grün E. 2007. Interstellar dust in the solar system. *Space Science Reviews* 130:401–408, doi:10.1007/s11214-007-9181-7.
- Landgraf M. 2000. Modeling the motion and distribution of interstellar dust inside the heliosphere. *Journal of Geophysical Research* 105:10303–10316.
- Landgraf M., Müller M., and Grün E. 1999. Prediction of the in-situ dust measurements of the Stardust mission to comet 81P/Wild 2. *Planetary and Space Science* 47:1029–1050.
- Lascelles S. F. and Armes S. P. 1995. Synthesis and characterisation of micrometer-sized polypyrrole-coated polystyrene latexes. *Advanced Materials* 7:864–866.
- Mocker A., Bugiel S., Auer S., Baust G., Colette A., Drake K., Fiege K., Grün E., Heckmann F., Helfert S., Hillier J. K., Kempf S., Matt G., Mellert T., Otto K., Postberg F., Röser H.-P., Shu A., Sternovsky Z., and Srama R. 2011. A 2MV Van de Graaff accelerator as a tool for planetary and impact physics research. *Review of Scientific Instruments* 82:095111, doi:10.1063/1.3637461.
- Ormond-Prout J., Dupin D., Armes S. P., Foster N. J., and Burchell M. J. 2009. Synthesis and characterization of polypyrrole-coated poly (methyl methacrylate) latex particles. *Journal of Material Chemistry* 19:1433–1442, doi:10.1039/B816839C.
- Price M. C., Kearsley A. T., Burchell M. J., Hörz F., Borg J., Bridges J. C., Cole M. J., Floss C., Graham G., Green S. F., Hoppe P., Leroux H., Marhas K. K., Park N., Stroud R., Stadermann F. J., Telisch N., and Wozniakiewicz P. J. 2010. Comet 81P/Wild 2: The size distribution of finer (sub-10 μm) dust collected by the Stardust spacecraft. *Meteoritics & Planetary Science* 45:1409–1428, doi:10.1111/j.1945-5100.2010.01104.x.
- Srama R. and Auer S. 2008. Low-charge detector for the monitoring of hyper-velocity micron-sized dust particles. *Measurement Science and Technology* 19:055203. doi:10.1088/0957-0233/19/5/055203.
- Sterken V. J., Westphal A. J., Altobelli N., Grün E., Hillier J. K., Postberg F., Srama R., Allen C., Anderson D., Ansari A., Bajt S., Bastien R. S., Bassim N., Bechtel H. A., Borg J., Brenker F. E., Bridges J., Brownlee D. E., Burchell M., Burghammer M., Butterworth A. L., Changela H., Cloetens P., Davis A. M., Doll R., Floss C., Flynn G., Frank D., Gainsforth Z., Heck P. R., Hoppe P., Hudson B., Huth J., Hvide B., Kearsley A., King A. J., Lai B., Leitner J., Lemelle L., Leroux H., Leonard A., Lettieri R., Marchant W., Nittler L. R., Oglione R., Ong W. J., Price M. C., Sandford S. A., Tresseras J. S., Schmitz S., Schoonjans T., Silversmit G., Simionovici A., Sole V. A., Stephan T., Stodolna J., Stroud R. M., Sutton S., Trieloff M., Tsou P., Tsuchiyama A., Tyliczszak T., Vekemans B., Vincze L., Korff J. V., Wordsworth N., Zevin D., and Zolensky M. E. 2014. Stardust Interstellar Preliminary Examination X: Impact speeds and directions of interstellar grains on the Stardust dust collector. *Meteoritics & Planetary Science*, doi:10.1111/maps.12219.
- Stroud R. M., Allen C., Ansari A., Anderson D., Bajt S., Bassim N., Bastien R. S., Bechtel H. A., Borg J., Brenker F. E., Bridges J., Brownlee D. E., Burchell M., Burghammer M., Butterworth A. L., Changela H., Cloetens P., Davis A. M., Doll R., Floss C., Flynn G., Frank D. R., Gainsforth Z., Grün E., Heck P. R., Hillier J. K., Hoppe P., Huth J., Hvide B., Kearsley A., King A. J., Kotula P., Lai B., Leitner J., Lemelle L., Leroux H., Leonard A., Lettieri R., Marchant W., Nittler L. R., Oglione R., Ong W. J., Postberg F., Price M. C., Sandford S. A., Tresseras J. S., Schmitz S., Schoonjans T., Silversmit G., Simionovici A. S., Sole V. A., Srama R., Stephan T., Sterken V. J., Stodolna J., Stroud R. M., Sutton S., Trieloff M., Tsou P., Tsuchiyama A., Tyliczszak T., Vekemans B., Vincze L., Korff J. V., Wordsworth N., Zevin D., and Zolensky M. E. 2014. Stardust Interstellar Preliminary Examination XI: Identification and elemental analysis of impact craters on Al foils from the Stardust interstellar dust collector. *Meteoritics & Planetary Science*, doi:10.1111/maps.12136.
- Tsou P., Brownlee D. E., Anderson J. D., Bhaskaran S., Chevront A. R., Clark B. C., Duxbury T., Economou T., Green S. F., Hanner M. S., Hörz F., Kissel J., McDonnell J. A. M., Newburn R. L., Ryan R. E., Sandford S. A., Sekanina Z., Tuzzolino A. J., Vellinga J. M., and Zolensky M. E. 2004. Stardust encounters comet 81P/Wild 2. *Journal of Geophysical Research* 109:E12S01/1-8. doi:10.1029/2004JE002317.
- Westphal A. J., Allbrink A., Allen C., Bajt S., Bastien R., Bechtel H., Bleuet P., Borg J., Sowker S., Brenker F., Bridges J., Brownlee D. E., Burchell M., Burghammer M., Butterworth A. L., Campanile A., Cloetens P., Cody G., Ferroir T., Ferrari K., Floss C., Flynn G. J., Frank D., Gainsforth Z., Grün E., Harmer M., Hoppe P., Kearsley A., Kulkami S., Lai B., Lemelle L., Leroux H., Lettieri R., Marchant W., McCreadie B., Nittler L. R., Oglione R., Postberg F., Rigamonti C., Sandford S. A., Schmitz S., Silversmit G., Simionovici A., Sperry G., Srama R., Stadermann F., Stephan T., Stroud R. M., Susini J., Sutton S., Thompson V., Toucoulou R., Trieloff M., Tsou P., Tsuchiyama A., Tyliczszak T., Vekemans B., Vincze L., Warren J., Yahnke T., Zevin D., and Zolensky M. E. 2010. Non-destructive search for interstellar dust using synchrotron microprobes. *AIP Conference Proceedings* 1221:131–138.
- Westphal A. J., Anderson D., Butterworth A. L., Frank D. R., Hudson B., Lettieri R., Marchant W., Korff J. V., Zevin D., Ardizzone A., Campanile A., Capraro M., Courtney K., Crumpler D., Cwik R., Gray F. J., Imada G., Karr J., Lau Wan Wah L., Mazzucato M., Motta P. G., Spencer R. C., Woodrough S. B., Santoni I. C., Sperry G., Terry J., Wordsworth N., Yanke Sr. T., Allen C., Ansari A., Bajt S., Bastien R. S., Bassim N., Bechtel H. A., Borg J., Brenker F. E., Bridges J., Brownlee D. E., Burchell M., Burghammer M., Changela H., Cloetens P., Davis A. M., Doll R., Floss C., Flynn G., Gainsforth Z., Grün E., Heck P. R., Hillier J. K., Hoppe P., Huth J., Hvide B., Kearsley A., King A. J., Lai B., Leitner J., Lemelle L., Leroux H., Leonard A., Nittler L. R., Oglione R., Ong W. J., Postberg F., Price M. C., Sandford S. A., Tresseras J. S., Schmitz S., Schoonjans T., Silversmit G., Simionovici A. S., Sole V. A., Srama R., Stephan T., Sterken V. J., Stodolna J., Stroud R. M., Sutton S., Trieloff M., Tsou P., Tsuchiyama A., Tyliczszak T., Vekemans B., Vincze L., and Zolensky M. E. 2014. Stardust Interstellar Preliminary Examination I: Identification of tracks in aerogel. *Meteoritics & Planetary Science*, doi:10.1111/maps.12168.
- Zolensky M. E., Zega T. J., Yano H., Wirick S., Westphal A. J., Weisberg M. K., Weber I., Warren J. L., Velbel M. A., Tsuchiyama A., Tsou P., Toppani A., Tomioka N., Tomeoka K., Teslich N., Taheri M., Susini J., Stroud R., Stephan T., Stadermann F. J., Snead C. J., Simon S. B.,

Simionovici A., See T. H., Robert F., Rietmeijer F. J. M., Rao W., Perronnet M. C., Papanastassiou D. A., Okudaira K., Ohsumi K., Ohnishi I., Nakamura-Messenger K., Nakamura T., Mostefaoui S., Mikouchi T., Meibom A., Matrajt G., Marcus M. A., Leroux H., Lemelle L., Le L., Lanzirotti A., Langenhorst F., Krot A. N., Keller L. P., Kearsley A. T., Joswiak D., Jacob D., Ishii H., Harvey R., Hagiya K., Grossman L., Grossman

J. N., Graham G. A., Gounelle M., Gillet P., Genge M. J., Flynn G., Ferroir T., Fallon S., Ebel D. S., Dai Z. R., Cordier P., Clark B., Chi M., Butterworth A. L., Brownlee D. E., Bridges J. C., Brennan S., Brearley A., Bradley J. P., Bleuet P., Bland P. A., and Bastien R. 2006. Mineralogy and petrology of comet 81P/Wild 2 nucleus samples. *Science* 314:1735–1739, doi:10.1126/science.1135842.
